Doping of Bi_2Te_3 using electron irradiation

C. W. Rischau,[1] B. Leridon,[2] B. Fauqué,[2] V. Metayer,[1] and C. J. van der Beek[1,*]

[1]*Laboratoire des Solides Irradiés (CNRS-CEA/DSM/IRAMIS), Ecole Polytechnique, 91128 Palaiseau Cedex, France*

[2]*Laboratoire de Physique et d'Etude des Matériaux (UPMC-CNRS), Ecole Supérieure de Physique et de Chimie Industrielles, 10 rue Vauquelin, 75005 Paris Cedex 05, France*

(Received 2 October 2013; published 19 November 2013)

Electron irradiation is investigated as a way to dope the topological insulator Bi_2Te_3. For this, p-type Bi_2Te_3 single crystals have been irradiated with 2.5 MeV electrons at room temperature and electrical measurements have been performed *in situ* as well as *ex situ* in magnetic fields up to 14 T. The defects created by irradiation act as electron donors, allowing the compensation of the initial hole-type conductivity of the material as well as the conversion of the conductivity from p to n type. The changes in carrier concentration are investigated using the Hall effect and Shubnikov–de Haas (SdH) oscillations, clearly observable in the p-type samples before irradiation, but also after the irradiation-induced conversion of the conductivity to n type. The SdH patterns observed for the magnetic field along the trigonal axis can be entirely explained assuming the contributions of only one valence and one conduction band, respectively, and Zeeman splitting of the orbital levels.

DOI: 10.1103/PhysRevB.88.205207 PACS number(s): 61.80.−x, 71.18.+y, 71.70.Ej

I. INTRODUCTION

Bismuth telluride Bi_2Te_3 is a narrow-band-gap semiconductor [energy gap $E_g = 0.13$ eV (Ref. 1)] which has been extensively studied because of its excellent thermoelectric properties. Recently, it has been discovered that Bi_2Te_3 as well as Bi_2Se_3 and Sb_2Te_3 belong to a group of materials called three-dimensional strong topological insulators (TIs).[2–4] Surprisingly, these were predicted to be insulating in the bulk, while their surface hosts topologically protected metallic states that can be described as massless Dirac fermions. These conducting surface states were first observed using surface-sensitive methods like angle-resolved photoemission spectroscopy[5] or scanning tunneling microscopy.[6] However, finding unambiguous evidence of the surface states using transport experiments has proven to be difficult. Namely, in most TI samples charge transport is dominated by a high bulk conductivity due to residual carriers arising from self-doping by point defects in the material, which complicates the identification of the surface contribution to the conductivity.[7–9] So far, successful approaches to suppressing the bulk conductivity include chemical doping,[8] electrical gating,[10] or the increase of the surface-to-volume ratio by fabricating thin films or nanowires.[11] However, if any future applications of TIs in technology are to be realized, achieving an insulating bulk state in these materials remains a necessary challenge. Here, we investigate electron irradiation-induced defects as a method to reduce the bulk conductivity of the topological insulator Bi_2Te_3.

Bi_2Te_3 has a tetradymite crystal structure [space group D^5_{3d} ($R\bar{3}m$)] with a rhombohedral primitive unit cell which contains five atoms in total, two Bi atoms on equivalent sites and three Te atoms which are distributed on two nonequivalent sites denoted Te1 and Te2. Bi_2Te_3 has a layered structure and can be described as a stack of so-called *quintuple layers* along the trigonal axis, which each contain five atomic layers in a Te1-Bi-Te2-Bi-Te1 pattern. The bonding between the Te1 layers belonging to two adjacent quintuple layers is of van der Waals type, whereas the bonding within the quintuple layers is covalent. The carrier type in Bi_2Te_3 depends strongly on the intrinsic point defects present in the material. It is generally accepted that the most prominent point defects in as-grown Bi_2Te_3 are the Bi_{Te1}, Bi_{Te2}, and Te_{Bi} antisite defects, with Bi_{Te1} and Bi_{Te2} acting as acceptors, whereas Te_{Bi} acts as an electron donor.[12] Te vacancies were predicted to act as double donors whereas Bi vacancies act as triple acceptors.[13] However, due to a higher formation energy of vacancies compared to Bi and Te antisite defects during growth of Bi_2Te_3 crystals, the doping during growth has been predicted to be almost entirely determined by the antisite defects.[12]

Both the top of the highest valence band and the bottom of the lowest conduction band of Bi_2Te_3 are generally described by a six-valley model with nonparabolic hole and electron pockets, respectively, which are located pairwise in the three mirror planes of the Brillouin zone containing the bisectrix and trigonal axis.[14,15] Thus, the effective mass tensor and the electric transport properties are expected to be highly anisotropic. Köhler determined the inverse effective-mass tensor $\boldsymbol{\alpha} = \alpha_{ij}/m_e$ (m_e is the free-electron mass) from Shubnikov–de Haas (SdH) oscillations by applying an ellipsoidal six-valley model for the valence-band edge [$\alpha_{11} = 32.5$, $\alpha_{22} = 4.81$, $\alpha_{33} = 9.02$, and $\alpha_{23} = 4.15$ (Ref. 16)] and the conduction-band edge [$\alpha_{11} = 46.9, \alpha_{22} = 5.92, \alpha_{33} = 9.5$, and $\alpha_{23} = 4.22$ (Ref. 17)] with axes 1, 2, and 3 referring to the binary **n**, bisectrix **s**, and trigonal axis **c**, respectively. Moreover, from the observation of a second SdH oscillation period for $\mathbf{B} \parallel \mathbf{c}$ on p-type samples with hole densities higher than 4×10^{18} cm^{-3}, it has been concluded that a second six-valley valence band, located 15–20 meV below the highest valence band, is filled for this range of hole densities.[16,18,19]

Previous irradiation studies on Bi_2Te_3 have been carried out using 7.5 MeV protons at room temperature,[20,21] or 5 MeV electrons at 250 K.[22] Hall-effect measurements on the irradiated samples have shown that it is in fact possible to convert the conduction of initially p-type Bi_2Te_3 to n type using irradiation-induced defects. From proton irradiations of Bi_2Te_3, Chaudhari and Bever estimated the threshold displacement energy E_d for a lattice atom to be in the range of 7.5–12.5 eV for Te1 atoms and 15–25 eV for Te2 and Bi atoms.[20] It was argued that the displacement

threshold for Te1 atoms is lower than for Te2 or Bi atoms because of the weaker van der Waals bonding between Te1 layers compared to the stronger covalent bonding within the quintuple layers. Annealing at 350 K of samples displaying n-type conduction after irradiation was found to restore the initial p-type conduction.[22]

We have irradiated p-type Bi_2Te_3 single crystals at room temperature with 2.5 MeV electrons, and studied the compensation of the acceptor-type defects by monitoring the resistivity of the samples *in situ* during irradiation. Changes in carrier density were deduced from *ex situ* magnetoresistance measurements in fields up to 14 T, by analyzing the Hall effect and SdH oscillations, detected for all irradiation doses in both the p- and n-type regimes. This, together with the excellent agreement of the extracted carrier effective masses and Fermi energies with those measured on Bi_2Te_3 doped by chemical means,[16,17] attests to the fact that doping is the main effect of the irradiation, and that charge carrier scattering is secondary. Moreover, the analysis of the SdH effect allows a coherent interpretation of the Fermi surface in p- and n-type Bi_2Te_3 in terms of a six-valley model and Zeeman splitting, without the need to invoke the contribution of either a second valence or conduction band or surface carriers.

II. METHODS

p-type Bi_2Te_3 single crystals (see Ref. 23 for fabrication details) were cut into bars with lateral dimensions of 1×3 mm^2 using a wire saw and then thinned down to a thickness of 10 to 40 μm using Scotch tape. Gold contact pads were evaporated on freshly cleaved surfaces, and contacted using silver paint and Au wires. All samples were irradiated at room temperature with 2.5 MeV electrons at the SIRIUS Pelletron accelerator facility of the Laboratoire des Solides Irradiés. The four-probe resistance of the samples was measured *in situ* during irradiation using an ac technique. After irradiation the samples were stored in liquid nitrogen to prevent any long-term annealing. They were then measured *ex situ* between 1.9 and 300 K using a Quantum Design 14 T physical properties measurement system. All measurements were performed with the magnetic field oriented along **c**. Prior to irradiation, all samples showed a similar temperature and field dependence of resistivity and Hall coefficient, differences in the absolute values being due to the uncertainty in the determination of the contact distances. In order to compare all samples, their initial resistivity has been normalized to the average resistivity of all unirradiated samples.

III. RESULTS AND DISCUSSION

A. Resistivity and low-field Hall effect

Figure 1(a) shows the resistance of a Bi_2Te_3 single crystal measured *in situ*, normalized to the initial resistance measured before irradiation, as a function of electron dose Q. The resistance first increases linearly up to a dose of around 50 mC/cm^2 until it reaches a maximum of 1.5–1.6 times its initial value at $Q \approx 80$–90 mC/cm^2. With further irradiation, the resistance decreases again, nearly reaching its initial value at a dose of 370 mC/cm^2. A similar behavior was observed for several samples irradiated to different total doses Q. For these, only the last points of the measured $R(Q)/R(Q=0)$ curves are shown in Fig. 1(a).

Figure 1(b) shows the resistivity of the irradiated samples as well as that of an unirradiated sample as a function of temperature. The resistivity of the virgin sample shows the metallic temperature dependence expected for p-type Bi_2Te_3, i.e., ρ_{xx} decreases with decreasing temperature. For the samples irradiated to total doses of 8.5, 23, and 43 mC/cm^2, ρ_{xx} still displays a metallic temperature dependence, even if the absolute values of the resistivity are increased over the entire temperature range. After irradiation with 86 mC/cm^2 the material is near optimum compensation and ρ_{xx} shows a more complicated temperature dependence. It first increases with decreasing T and reaches a maximum at around 160 K, before decreasing to a resistivity of 12 mΩ cm at 1.9 K, which corresponds to an increase by approximately two orders of magnitude compared to the virgin sample. It should be noted that this value of $\rho_{xx}(1.9\ \mathrm{K})$ is comparable to that obtained on nonmetallic Bi_2Te_3 samples (12 mΩ cm) cut from crystals grown with a weak compositional gradient[7] or lightly doped $Bi_{2-x}Tl_xTe_3$ samples (28 mΩ cm for $x = 0.1$).[24] However, it is much lower than that obtained for heavy chemical doping in $Bi_2Te_{3-x}Se_x$ (1 Ω cm for $x = 0.9$–1).[8,25] After further irradiation to 130 mC/cm^2, ρ_{xx} shows a similar temperature dependence, but compared to the sample irradiated with 86 mC/cm^2, the absolute values of the resistivity have decreased again over the entire investigated temperature region. For samples irradiated to doses higher than 190 mC/cm^2, ρ_{xx} shows again a metallic temperature dependence below 260 K.

Figure 1(c) shows the low-field Hall coefficient R_H as a function of temperature, determined from the slope $\frac{\Delta\rho_{yx}}{\Delta B}$ of the Hall resistivity ρ_{yx} around zero field ($-0.2 \lesssim B \lesssim 0.2$ T) using a linear fit. The virgin sample displays a positive and almost temperature-independent $R_H(T)$. After irradiation up to $Q = 86$ mC/cm^2, R_H is still positive over the entire temperature range, but now increases linearly with decreasing T up to a value of 6.5 cm^3/C at 1.9 K, even if the value at room temperature remains nearly the same as for the virgin sample. After irradiation with 130 mC/cm^2, R_H has changed sign, i.e., the conduction has changed from p to n type. With further irradiation R_H increases, but remains negative.

In the case of an anisotropic Fermi surface, the Hall carrier density n_H is given by the low-field Hall coefficient R_H via $n_H = ra/(eR_H)$ with the Hall scattering factor r and an anisotropy factor a. The factor ra has been estimated by Drabble from galvanomagnetic measurements as $ra = 0.514$ and 0.32 for p- and n-type Bi_2Te_3, respectively.[14,15] It should be noted that, since $ra \to 1$ for high magnetic fields, one can alternatively use the high-field saturation value R_H^∞ of the Hall coefficient (if determinable) to calculate the carrier density $n_H^\infty = 1/(eR_H^\infty)$, as has been done in previous works on Bi_2Te_3.[16–19,26,27] Comparison of the carrier densities calculated from the low- and high-field Hall coefficients given in Table I confirms that the two are comparable. Figures 1(d) and 1(e) show the Hall carrier density $|n_H|$ and the Hall mobility $\mu_H = 1/(en_H\rho_{xx})$, respectively, as function of temperature. The virgin sample shows a nearly temperature-independent n_H. After irradiation with 86 mC/cm^2, $n_H(T = 1.9\ \mathrm{K})$ decreased to 5.0×10^{17} cm^{-3}, i.e., a decrease of one order of magnitude compared to the value in the unirradiated

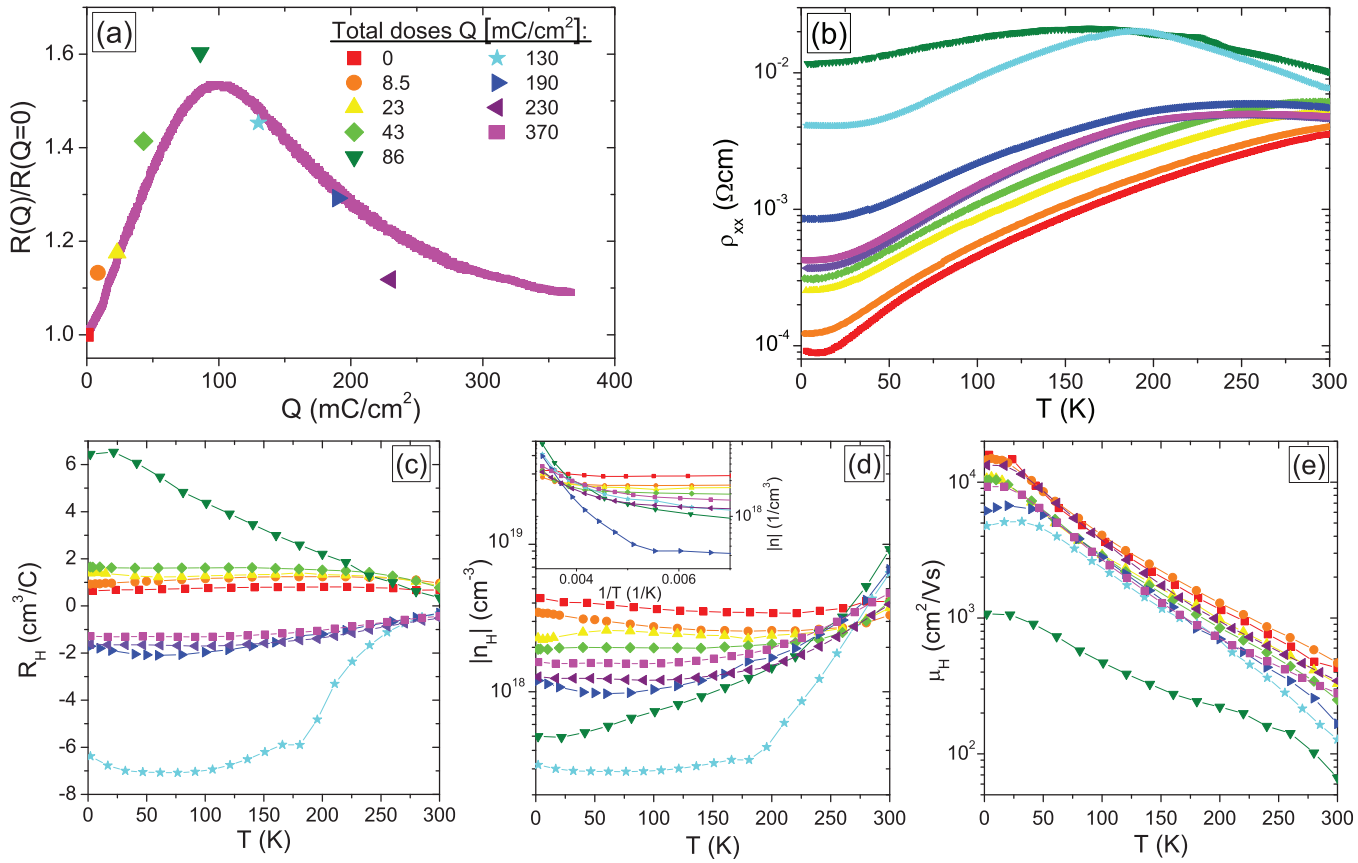

FIG. 1. (Color online) (a) Normalized resistance $R(Q)/R(Q=0)$ of a Bi_2Te_3 single crystal, measured *in situ* during 2.5 MeV electron irradiation at room temperature, as a function of electron dose Q (magenta squares). The different other symbols represent the $R(Q)/R(Q=0)$ values obtained for different samples, irradiated to different total doses Q. (b) Resistivity ρ_{xx} and (c) low-field Hall coefficient R_H of the same samples measured *ex situ* as function of temperature T. (d) Absolute values of the Hall carrier concentration $|n_H|$ and (e) the Hall mobility μ_H, both calculated assuming only one carrier type. The inset of (d) shows $|n_H|$ as a function of $1/T$.

sample, 4.3×10^{18} cm^{-3}. However, it should be noted that $n_H = ra/(eR_H)$ does not give the exact carrier concentration for samples near optimum compensation, since two types of carriers with comparable concentrations are present in this region. The inset in Fig. 1(d) diplays $|n_H|$ as a function of $1/T$ for high temperatures. For temperatures above 280–300 K, n_H seems to show an activated behavior which is the most pronounced for samples irradiated to 86 and 130 mC/cm^2, i.e.,

TABLE I. Overview of the carrier concentrations n_H and n_H^∞ obtained from the low- and high-field Hall coefficients at 1.9 K as well as the parameters obtained from temperature and field dependence of the oscillation amplitude measured at 1.9 K for **B** ∥ **c** (n.d. indicates parameter nondeterminable due to a too limited number of oscillation maxima). The m_z values were not determined experimentally, but were calculated from the effective mass tensors given in Refs. 16 and 17 for p- and n-type Bi_2Te_3, respectively. The values of $6n_{SdH}$, the spin-splitting factor M, and the g factor were determined by simulations based on Eq. (3).

	Hall effect		Temperature dependence and Dingle analysis					Fit			
Q (mC/cm^2)	n_H (10^{18} cm^{-3})	n_H^∞	$\Delta(1/B)$ (1/T)	m_c (units of m_e)	ϵ_F (meV)	τ_D (10^{-13} s)	T_D (K)	m_z (units of m_e)	$6n_{SdH}$ (10^{18} cm^{-3})	M	g
0	4.3	4.6	0.052 ± 0.0005	0.107 ± 0.01	21 ± 1	1.8 ± 0.2	6.5 ± 0.4	0.244	4.2	0.67,1.33	12.5,24.9
8.5	3.5	3.8	0.058 ± 0.0005	0.101 ± 0.01	20 ± 2	1.2 ± 0.1	10 ± 0.5	0.228	3.7	0.67,1.33	13.3,26.3
23	2.3	2.8	0.067 ± 0.001	0.094 ± 0.005	18 ± 1	0.97 ± 0.05	12.5 ± 0.7	0.214	2.9	0.67,1.33	14.3,28.3
43	1.9	1.7	0.078 ± 0.002	0.09 ± 0.01	16 ± 2	0.72 ± 0.1	15 ± 2	0.178	2.2	0.69,1.31	15.3,29.1
86	0.5	0.9	n.d.	n.d.	n.d.	n.d.	n.d.				
130	−0.31	n.d.	n.d.	n.d.	n.d.	n.d.	n.d.				
190	−1.2	−2.1	n.d.	n.d.	n.d.	n.d.	n.d.				
230	−1.3	−2.1	0.089 ± 0.002	n.d.	n.d.	n.d.	n.d.	0.167	2.0	0.57,1.43	17.5,44
370	−1.6	−2.4	0.087 ± 0.002	n.d.	n.d.	n.d.	n.d.	0.167	2.1	0.57,1.43	17.5,44

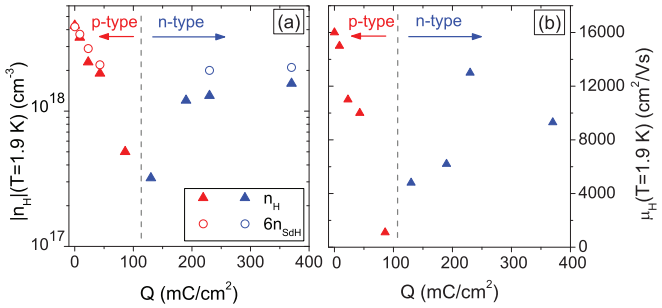

FIG. 2. (Color online) (a) Absolute value of the carrier concentrations n_H and $6n_{SdH}$ obtained from low-field Hall effect and SdH oscillations at 1.9 K, respectively, as a function of dose Q. (b) Hall mobility μ_H at 1.9 K as a function of Q.

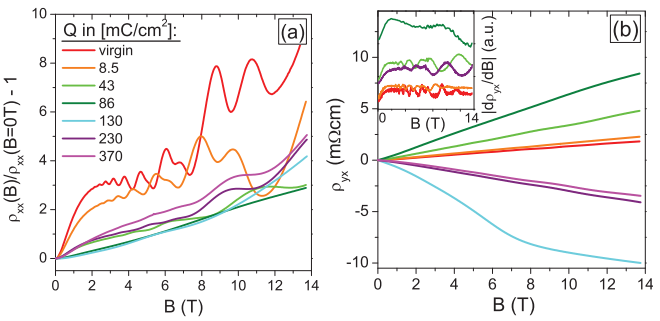

FIG. 3. (Color online) (a) Normalized magnetoresistance $\rho_{xx}(B)/\rho_{xx}(B=0\,\mathrm{T})-1$ measured at 1.9 K as a function of magnetic field B after different total irradiation doses Q. (b) Hall resistivity ρ_{yx} at 1.9 K as a function of B with the inset showing $\left|d\rho_{yx}/dB\right|$ vs B.

the region of activated behavior extends to lower T. However, an upper temperature limit of 300 K for the measurements is not high enough in order to reliably determine values for the activation energies. Since an annealing of electron-irradiated defects at 350 K has been reported,[22] we have not measured our samples at temperatures higher than 300 K. Figures 2(a) and 2(b) show n_H and μ_H at 1.9 K as a function of Q. Both n_H and μ_H decrease as one approaches the dose of optimal compensation. Interestingly, μ_H increases again once the conduction has changed to n type. A similar dependence of the mobility as a function of dose, i.e., carrier concentration, was observed during irradiation of PbSnTe (Ref. 28) and $Hg_{1-x}Cd_xTe$ (Ref. 29) and was explained with a model based on ionized impurity scattering.

B. High-field magnetoresistance

Figure 3(a) depicts the normalized magnetoresistance $\rho_{xx}(B)/\rho_{xx}(B=0\ \mathrm{T})-1$ as function of magnetic field B for the virgin and selected irradiated samples at 1.9 K. The normalized magnetoresistance of the unirradiated sample shows a nonlinear background with a superimposed pattern of Shubnikov–de Haas oscillations. For irradiation up to 86 mC/cm^2, the normalized magnetoresistance decreases as a function of electron dose and the background becomes more linear. The oscillations become less pronounced, yet changes regarding the positions and the period of the oscillations are clearly visible. After irradiation doses of 130 mC/cm^2 and higher, the normalized magnetoresistance increases again and still shows an almost linear B dependence. Furthermore, the SdH oscillations seem to reappear, i.e., become more pronounced again.

The Hall resistivity ρ_{yx} as a function of B, depicted in Fig. 3(b), shows a linear background at magnetic fields $B \gtrsim 1$ T on which SdH oscillations are superposed. However, for small magnetic fields up to $B \lesssim 1$ T, ρ_{yx} has a parabolic field dependence, which can be seen in the plot of $\left|d\rho_{yx}/dB\right|$ vs B [see the inset of Fig. 3 (b)]. This nonlinearity of $\rho_{yx}(B)$ has been previously reported for p-type Bi_2Te_3, but only for hole densities higher than 4×10^{18} cm^{-3}, and has been attributed to the presence of a second valence band for these carrier densities.[16,22] It should be noted that we observe this nonlinearity for all n- and p-type samples independent of irradiation dose, i.e., for hole densities in the range of $n \approx (0.5\text{–}4.3)\times10^{18}$ cm^{-3}. Therefore, we propose that the observed nonlinearity is not due to a different type of hole originating from a second valence band, but to the strong anisotropy of the Fermi surface.

C. Shubnikov–de Haas oscillations

Figure 4(a) shows the resistivity ρ_{xx} at 1.9 K after subtraction of a smooth background as a function of $1/B$ for different irradiation doses. The unirradiated p-type sample shows very pronounced SdH oscillations with a double-peak structure at low $1/B$ values, due to either Zeeman splitting or the superposition of a second oscillation frequency. Assuming a six-valley structure for the highest valence band,[16] only one oscillation frequency is expected for $\mathbf{B} \parallel \mathbf{c}$ whereas for $\mathbf{B} \parallel \mathbf{s}$ or $\mathbf{B} \parallel \mathbf{n}$ two different oscillation frequencies should arise. We propose that the observed splitting for $\mathbf{B} \parallel \mathbf{c}$ on our samples (hole densities below 4×10^{18} cm^{-3}) is due to Zeeman splitting. It should be noted that the appearance of a second oscillation frequency for $\mathbf{B} \parallel \mathbf{c}$ has been previously observed for hole densities above 4×10^{18} cm^{-3} and ascribed to the contribution of a second six-valley valence band.[16,19] Assuming Zeeman splitting, the periodicity of the SdH pattern can be well described with a single oscillation period of $\Delta(1/B) = 0.052$ 1/T, with the multiples of $\Delta(1/B)$ [see the vertical grid lines in Fig. 4(a)] exactly centered between split peaks.

With increasing dose, i.e., decreasing carrier density, the peaks corresponding to higher Landau levels (LLs) become less visible due to both the decrease of the Fermi energy and the increase of irradiation-induced lattice disorder. For the p-type samples up to total doses of 43 mC/cm^2, the periodicity of the SdH pattern can always be described by one single oscillation period $\Delta(1/B)$ that increases with irradiation dose, i.e., decreasing hole concentration (see Table I). Even if the peak splitting at lower $1/B$ values becomes less visible with increasing dose, it can be observed for all p-type samples up to 43 mC/cm^2. For the samples irradiated to 86 and 130 mC/cm^2 one observes just one oscillation maximum and minimum, respectively, which makes analysis impossible. It should be noted that, the mobility estimated from the low-field Hall effect $\mu_H(1.9\ \mathrm{K}) = 1100$ cm^2/Vs (see Fig. 2) is still quite high for the sample near optimum compensation ($Q = 86$ mC/cm^2). Interestingly, after further irradiation to 230 and 370 mC/cm^2, i.e., increasing electron carrier concentration, a larger number

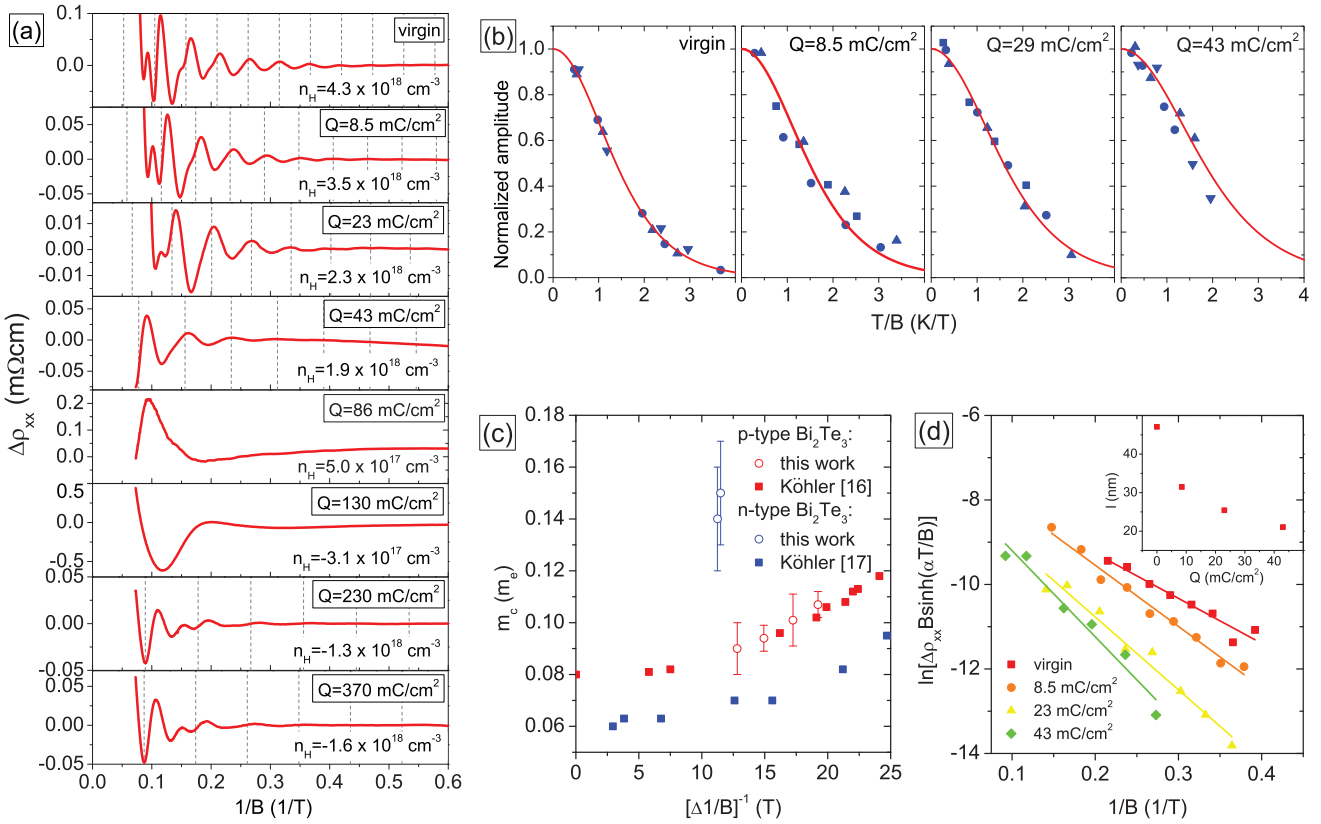

FIG. 4. (Color online) (a) Oscillating part of the resistivity $\Delta\rho_{xx}$ at 1.9 K for $\mathbf{B} \parallel \mathbf{c}$ as a function of inverse magnetic field $1/B$ for different irradiation doses. For each dose, the vertical gray grid lines indicate the multiples of the oscillation periods $\Delta(1/B)$ given in Table I. (b) Temperature dependence of the oscillation amplitude with solid lines representing the fits obtained using Eq. (2). Different symbols correspond to the analysis of different LLs, i.e., peaks at different $1/B$ positions. In order to compare the temperature dependence of different peaks, the oscillation amplitudes have been normalized to the value of the fit for $1/B \to 0$. (c) Cyclotron masses m_c as function of the inverse oscillation period $[\Delta(1/B)]^{-1}$. (d) Dingle plots at $T = 1.9$ K and inset showing the mean free path l as a function of dose Q.

of maxima reappears. For the n-type samples, there seems to be either spin splitting, as in the case of the p-type samples, or, alternatively, the appearance of a second oscillation frequency due to the contribution of a second type of carrier.

The SdH period $\Delta(1/B)$ can be expressed as

$$\Delta\left(\frac{1}{B}\right) = \frac{2\pi e}{\hbar S_F} = \frac{e\hbar}{m_c \epsilon_F} \tag{1}$$

with S_F the cross section of the Fermi surface perpendicular to the direction of the field $\mathbf{B}$, m_c the cyclotron mass, $\hbar$ the Planck constant, and ϵ_F the Fermi energy (measured from the band edge). Using the standard Lifshitz-Kosevich theory,[30] the temperature dependence of the oscillation amplitude $\Delta\rho_{xx}$ of a fixed peak can be fitted as a function of T/B using

$$\Delta\rho_{xx}(T/B) = \alpha T/[B \sinh(\alpha T/B)] \tag{2}$$

with $\alpha = 2\pi^2 m_c k_b/(\hbar e)$, allowing for the extraction of m_c. Figure 4(b) shows the temperature dependence of the oscillation amplitude as well as the corresponding fits to Eq. (2) for the p-type samples for which this analysis was possible. As in Köhler's work, cyclotron masses determined from visibly split peaks showed a strong dependence on the $1/B$ position of the analyzed peak; therefore, only nonsplit peaks were used to determine m_c. The plot of m_c as a function of the inverse oscillation period $[\Delta(1/B)]^{-1}$ in Fig. 4(c) shows a decrease of m_c with decreasing $[\Delta(1/B)]^{-1}$, i.e., increasing dose and decreasing hole concentration, respectively. This confirms the nonparabolic energy dispersion $\epsilon(\mathbf{k})$ of the highest valence band in p-type Bi_2Te_3. Furthermore, Fig. 4(c) depicts the cyclotron masses found by Köhler on a series of p- and n-type samples with doping realized during crystal growth[16,17] showing a good agreement with the values found on our irradiated p-type samples. However, there is a strong deviation of the m_c values extracted from samples irradiated to 230 and 370 mC/cm^2. This probably stems from the error introduced by spin splitting of the analyzed peaks. Unlike in the work of Köhler, the higher nonsplit LLs are not visible.

The field dependence of the oscillation amplitude can be used to determine the Dingle scattering time τ_D by plotting $\ln[\Delta\rho_{xx} B \sinh(\alpha T/B)] \propto \pi m_c/(e\tau_D B)$ as a function of $1/B$ for a fixed T (a *Dingle plot*).[30] Figure 4(d) shows the Dingle plots for the unirradiated and some of the irradiated p-type samples at $T = 1.9$ K. For all other irradiated samples, the number of observed peaks was not sufficient to carry out this analysis. The scattering time τ_D corresponds to a Dingle temperature $T_D = \hbar/(2\pi k_B \tau_D)$ and can be used to estimate the mean free path $l = v_F \tau_D$ with v_F the Fermi velocity calculated from Eq. (1) and $\epsilon_F = \frac{1}{2} m_c v_F^2$. The mean free path as a function of Q is shown in the inset of Fig. 4(d) and seems

to saturate at about half of its initial value at $Q = 43$ mC/cm^2. It should be noted that, up to this dose, n_H also decreased by a factor of 2, indicating that the effects of disorder and the decrease of the Fermi energy are comparable in this dose range. All parameters obtained from the analysis of the temperature and field dependence of the oscillation amplitude are given in Table I.

Since the Fermi surfaces of p- and n-type Bi_2Te_3 are nonspherical and nonparabolic, an estimation of the carrier density n_{SdH} from the SdH oscillations is not obvious. In order to calculate n_{SdH} as well as to investigate the origin of the double-peak structure observed at high B, we use the following model including spin splitting to simulate the LL spectra (for details see the Appendix). In this model, the carrier density n_{SdH} of one single ellipsoidal hole or electron pocket is given by

$$n_{SdH} = \frac{1}{2\pi^2 l_B^2} \sum_{i=0}^{i_{\max}} \sum_{\pm M} \sqrt{\frac{2m_z}{\hbar^2}\left[\epsilon_F - \left(i + \frac{1}{2} \pm \frac{M}{2}\right)\hbar\omega_c)\right]} \tag{3}$$

with $l_B = \sqrt{\hbar/eB}$ and m_z the longitudinal mass. The spin-splitting factor $M = \frac{E_Z}{\hbar\omega_c} = g\frac{m_c}{2m_e}$ describes the ratio of the Zeeman energy E_Z to the cyclotron energy $\hbar\omega_c$ and is related to the g-factor g. The conductivity σ_{xx} is enhanced each time the Fermi energy crosses a LL. Therefore, the field positions of the σ_{xx} oscillation maxima are determined by the points of intersection between ϵ_F and the energy of the ith Landau level, given by $\epsilon_i = (i + \frac{1}{2} \pm \frac{M}{2})\hbar\omega_c$. Thus, one has to solve Eq. (3) numerically to calculate the Fermi energy $\epsilon_F = \epsilon_F(n_{SdH}, B)$. Since both the carrier concentration and the Fermi energy are unknown, we first assume a constant carrier concentration n_{SdH}, independent of B, and then adjust n_{SdH} as well as M simultaneously to match the measured SdH maxima of σ_{xx} with the intersections of LLs and the Fermi energy. As pointed out recently in a similar study on Bi_2Se_3, one has to be careful when using the oscillations of other quantities than σ_{xx} to compare with the calculated Landau spectrum.[31] In the case of $\rho_{yx} \gg \rho_{xx}$, the maxima of ρ_{xx} and σ_{xx} appear at the same fields whereas for comparable ρ_{xx} and ρ_{yx}, the maxima of ρ_{xx} and σ_{xx} do not coincide. Since in our case $\rho_{yx} \gg \rho_{xx}$ except for samples irradiated with 86 and 130 mC/cm^2, for which the number of observed maxima is not sufficient to perform this kind of analysis, we used ρ_{xx} to perform the analysis described above. For the p-type samples, we used the m_c extracted from the temperature dependence of $\Delta\rho_{xx}$ for the calculation of ϵ_F. Since a reliable determination of m_c for the two n-type samples ($Q = 230$ and 370 mC/cm^2, respectively) was not possible (see above), we used $m_c = 0.065$ based on the value found by Köhler[17] for comparable oscillation frequencies $\Delta(1/B)$. The longitudinal masses m_z were calculated using the effective-mass tensors and their dependence on ϵ_F found by Köhler[16,17] and are given in Table I (see the Appendix for more details).

Figure 5 shows the Fermi energy obtained using Eq. (3), together with the Landau levels and the measured $\Delta\rho_{xx}$ for the

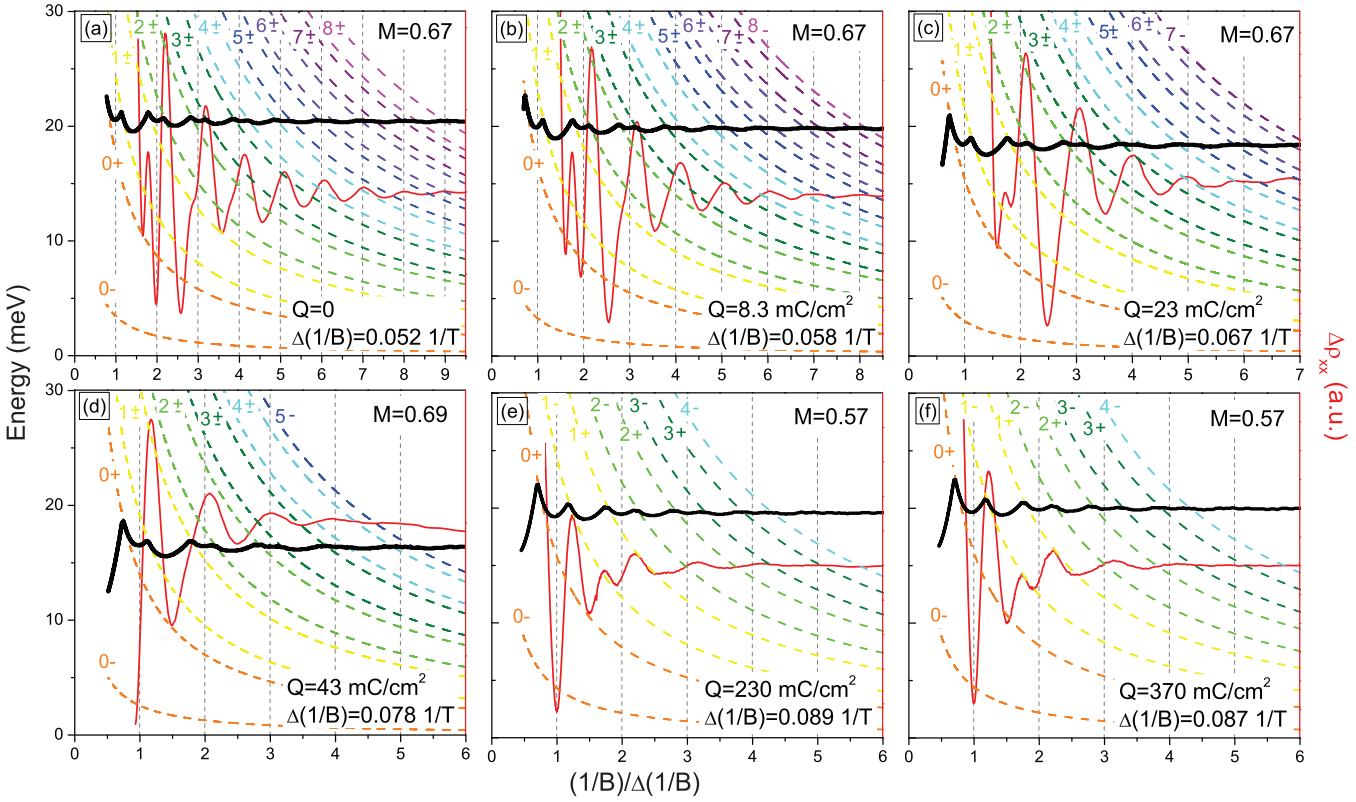

FIG. 5. (Color online) Fermi energy ϵ_F calculated with Eq. (3) (black line, left scale) and energy of the split Landau levels (colored lines with LL indices, left scale) as well as the oscillating part of the measured resistivity $\Delta\rho_{xx}$ (red line, right scale) as a function of $(1/B)/\Delta(1/B)$ for the virgin sample, as well as samples irradiated to different doses Q. The corresponding fitting parameters are given in Table I.

virgin and the irradiated samples for which this analysis was possible. It turns out that the positions of all maxima can be reproduced with good accuracy for all samples. In our model, the double-peak structure observed for the p-type samples thus originates from *Zeeman splitting*. For the p-type samples [see Figs. 5(a) to 5(d)], $M = 1 \pm 0.33$ is found, i.e., either $M = 0.67$ or 1.33, which agrees well with the value of $M = 0.61$ found by Köhler for the valence-band edge.[26] In order to make the distinction between $M = 0.67$ or 1.33, measurements at higher magnetic fields are necessary to attain the quantum limit and to observe the lowest LL with index $i = 0^-$. It should be noted that because the spin-splitting factor is larger than 0.5, the peaks at higher $1/B$ values that appear not to be split are in fact a superposition of the spin-up and spin-down levels of two adjacent LLs. However, due to the small amplitude $\Delta\rho_{xx}$, they appear as one single peak. Both n-type spectra could be well described assuming a spin splitting of $M = 1 \pm 0.43$, i.e., either $M = 0.57$ or 1.43, which again agrees with the value of $M = 0.53$ found by Köhler for the lowest conduction band.[27] However, since only the lower spin-split LLs are visible, the determination of M and n_{SdH} is less acccurate than in the case of the p-type samples. Comparison of the possible values for the g factor of Bi_2Te_3, calculated from the spin-splitting factor M (see Table I), shows that it lies in the same order of magnitude as the g factor in Bi_2Se_3, determined by Fauqué *et al*. to be $g = 14.3$ or 28.6, respectively.[31]

Assuming a six-valley model for both the highest valence and the lowest conduction bands, one has to multiply the obtained densities n_{SdH} by a factor of 6 in order to obtain the total carrier density. Comparison of the values for $6n_{SdH}$ with n_H or n_H^∞ obtained from the Hall effect shows good agreement (see Table I and Fig. 2). This, together with the good agreement of the simulated LL spectra with the measured SdH oscillations, suggests that the electric transport in our p- as well n-type Bi_2Te_3 can be explained in terms of one single valence and conduction band, respectively, and the presence of Zeeman splitting. However, for the samples close to optimal compensation ($Q = 86$ and 130 C/cm^2), two different types of carriers contribute to the conductivity.

IV. CONCLUSION

Recently, Bi_2Te_3 has attracted enormous attention as a topological insulator. However, regarding future applications of TIs, samples with an insulating bulk state are needed. We showed that it is possible to dope p-type Bi_2Te_3 in a very controlled manner using electron irradiation. The irradiation-induced defects partially compensate the Bi_{Te} antisite defects initially present in the material and convert the conduction from p to n type. Analysis of the Hall effect and Shubnikov–de Haas oscillations shows that the electrical transport in p- (hole densities above 4×10^{18} cm^{-3}) as well n-type (electron densities below 2.5×10^{18} cm^{-3}) Bi_2Te_3 can be understood in terms of one single valence and conduction band, respectively, and the presence of Zeeman splitting. This study solely concerns the doping of bulk Bi_2Te_3; none of the irradiated samples displayed any features associated with surface carriers. However, since doping of Bi_2Te_3 using electron irradiation seems possible, it would be extremely interesting to perform these kind of irradiations on thinner Bi_2Te_3 samples on which the surface states have already been identified before irradiation. Besides doping effects, irradiation of topological insulators could give new insight into the behavior of the surface states with respect to disorder, which up to now has been studied only theoretically.[32,33]

Under high-energy electron irradiation, lattice atoms can be displaced by electrons or secondary knock-on atoms, if the energy of the projectile exceeds the threshold displacement energy E_d of the different lattice atoms. Due to the high energy of the electrons of 2.5 MeV in the present study, the displacement of all different lattice atoms, i.e., Te1, Te2, and Bi, as well as the displacement of the atoms on antisites is expected. However, regarding the higher total number of Te sites (ratio 3:2) and the lower displacement threshold of Te1 atoms,[20] one can assume a larger number of displaced Te than Bi atoms. Since the irradiation temperature is relatively high, the displaced atoms as well as the created vacancies might form more stable interstitial or vacancy clusters or recombine with vacancies resulting in annihilation of defects or the creation of antisite defects. Both Hall-effect measurements and the analysis of the observed SdH oscillations clearly indicate the electron donor character of the irradiation-induced defects. Therefore, we assume Te vacancy clusters and Te_{Bi} antisite defects, both acting as electron dopants,[12,13] to be the predominant defects. Although the doping effect of Te and Bi interstitials has been less studied than the latter defects, Te interstitials have also been assumed to act as electron donors in a previous study on proton-irradiated Bi_2Te_3.[20] Transmission electron microscopy studies on these proton-irradiated samples showed the presence of interstitial and vacancy cluster.[21] However, further detailed studies of the defects created by room- and also low-temperature irradiation are necessary to fully understand the damage formation in Bi_2Te_3 under irradiation.

ACKNOWLEDGMENTS

We would like to thank A. Hruban, A. Wolos, and M. Kaminska for supplying the samples and the SIRIUS team for technical support. This work was partly supported through a SESAME grant from Region Ile-de-France.

APPENDIX: CALCULATION OF CARRIER DENSITY FROM SHUBNIKOV–DE HAAS OSCILLATIONS

The energy of electron states in the presence of a magnetic field $\mathbf{B} = (0,0,B)$ along the z direction is given by

$$\epsilon(i,k_z) = \left(i + \frac{1}{2} \pm \frac{M}{2}\right)\hbar\omega_c + \frac{\hbar^2}{2m_z}k_z^2 \qquad \text{(A1)}$$

with the cyclotron frequency $\omega_c = \frac{eB}{m_c}$, the cyclotron mass m_c, the longitudinal mass m_z, the spin-splitting factor $M = g\frac{m_c}{2m_0}$, and the g factor g. The cyclotron mass m_c can be described using the effective-mass tensor $\mathbf{m}$ or the inverse effective-mass tensor $\boldsymbol{\alpha} = \mathbf{m}^{-1}$ as $m_c = \sqrt{\det\mathbf{m}/m_z}$ with $m_z = \mathbf{b}\cdot\mathbf{m}\cdot\mathbf{b}$, where $\mathbf{b}$ is the unit vector of $\mathbf{B}$. In order to count the electronic states we assume a box in $\mathbf{k}$ space of volume V with sides L_x, L_y, and L_z. Each energy level fixed by (i,k_z) is p-fold degenerate with $p = \frac{m_c\omega_c}{2\pi}L_xL_y$.[34] The total number of carriers

N is the sum of the carriers on each Landau level i,

$$N = \sum_{i=0}^{i_{\max}} \sum_{\pm M} p N_{i,k_z}^{\pm M}, \tag{A2}$$

with $N_{i,k_z}^{\pm M}$ being the number of spin-up $(+M)$ and spin-down $(-M)$ carriers, respectively, on the ith Landau level. The index $i_{\max}$ of the highest occupied LL is given by $i_{\max} = \text{floor}(\frac{\epsilon_F}{\hbar\omega_c} - \frac{1}{2} \pm \frac{M}{2})$. The wave number k_z is quantized in units of $2\pi/L_z$ and varies for the ith Landau level in the range $-k_{z,\max}^i < k_z \leqslant k_{z,\max}^i$ with $k_{z,\max}^i = k_{z,\max}^i(\epsilon_F, \pm M) = \sqrt{\frac{2m_c}{\hbar^2}[\epsilon_F - (i + \frac{1}{2} \pm \frac{M}{2})\hbar\omega_c]}$ calculated from Eq. (A1).

Therefore, for each Landau level there are

$$N_{i,k_z}^{\pm M} = 2\,\frac{k_{z,\max}^i(\epsilon_F, \pm M)}{(2\pi/L_z)} \tag{A3}$$

allowed states for spin-up $(+M)$ and spin-down $(-M)$ carriers. The total carrier concentration n can then be calculated using Eq. (A2) and $n = N/V$,

$$n = \frac{1}{2\pi^2 l_B^2} \sum_{i=0}^{i_{\max}} \sum_{\pm M} \sqrt{\frac{2m_z}{\hbar^2}\left[\epsilon_F - \left(i + \frac{1}{2} \pm \frac{M}{2}\right)\hbar\omega_c\right]} \tag{A4}$$

with $l_B = \sqrt{\hbar/eB}$.

*Corresponding author: kees.vanderbeek@polytechnique.edu

[1] R. Sehr and L. R. Testardi, J. Phys. Chem. Solids **23**, 1219 (1962).
[2] J. E. Moore and L. Balents, Phys. Rev. B **75**, 121306(R) (2007).
[3] L. Fu, C. L. Kane, and E. J. Mele, Phys. Rev. Lett. **98**, 106803 (2007).
[4] L. Fu and C. L. Kane, Phys. Rev. B **76**, 045302 (2007).
[5] D. Hsieh, D. Qian, L. Wray, Y. Xia, Y. S. Hor, R. J. Cava, and M. Z. Hasan, Nature (London) **452**, 970 (2008).
[6] P. Roushan, J. Seo, C. V. Parker, Y. S. Hor, D. Hsieh, D. Qian, A. Richardella, M. Z. Hasan, R. J. Cava, and A. Yazdani, Nature (London) **460**, 1106 (2009).
[7] D.-X. Qu, Y. S. Hor, J. Xiong, R. J. Cava, and N. P. Ong, Science **329**, 821 (2010).
[8] Z. Ren, A. A. Taskin, S. Sasaki, K. Segawa, and Y. Ando, Phys. Rev. B **82**, 241306(R) (2010).
[9] A. A. Taskin, Z. Ren, S. Sasaki, K. Segawa, and Y. Ando, Phys. Rev. Lett. **107**, 016801 (2011).
[10] B. Sacépé, J. B. Oostinga, J. Li, A. Ubaldini, N. J. G. Couto, E. Giannini, and A. F. Morpugo, Nat. Commun. **2**, 575 (2011).
[11] H. Peng, K. Lai, D. Kong, S. Meister, Y. Chen, X.-L. Qi, S.-C. Zhang, Z.-X. Shen, and Y. Cui, Nat. Mater. **9**, 225 (2010).
[12] A. Hashibon and C. Elsässer, Phys. Rev. B **84**, 144117 (2011).
[13] P. Pecheur and G. Toussaint, J. Phys. Chem. Solids **55**, 327 (1994).
[14] J. R. Drabble, Proc. Phys. Soc. London **72**, 380 (1958).
[15] J. R. Drabble, R. D. Groves and R. Wolfe, Proc. Phys. Soc. London **71**, 430 (1958).
[16] H. Köhler, Phys. Status Solidi B **74**, 591 (1976).
[17] H. Köhler, Phys. Status Solidi B **73**, 95 (1976).
[18] A. von Middendorff and G. Landwehr, Solid State Commun. **11**, 203 (1972).
[19] V. V. Sologub, R. V. Parfen'ev, and A. D. Goletskaya, Pis'ma Zh. Éksp. Teor. Fiz. **21**, 711 (1975) [JETP Lett. **21**, 337 (1975)].
[20] P. Chaudhari and M. B. Bever, J. Appl. Phys. **37**, 4181 (1966).
[21] P. Chaudhari and M. B. Bever, J. Appl. Phys. **38**, 2417 (1967).
[22] A. E. Karkin, V. V. Shchennikov, B. N. Goshchitskii, S. E. Danilov, and V. L. Arbuzov, JETP **86**, 976 (1998).
[23] A. Hruban, A. Materna, W. Dalecki, G. Strzelecka, M. Piersa, E. Jurkiewicz-Wegner, R. Diduszko, M. Romaniec, and W. Orlowski, Acta Phys. Pol. A **120**, 950 (2011).
[24] H. Chi, W. Liu, K. Sun, X. Su, G. Wang, P. Lošt'ák, V. Kucek, Č. Drašar, and C. Uher, Phys. Rev. B **88**, 045202 (2013).
[25] A. Akrap, A. Ubaldini, E. Giannini, and L. Forró, arXiv:1210.3901.
[26] H. Köhler, Phys. Status Solidi B **75**, 441 (1976).
[27] H. Köhler, Phys. Status Solidi B **75**, 127 (1976).
[28] B. A. Green, J. Appl. Phys. **47**, 2243 (1976).
[29] B. A. Green, R. E. Leadon, and C. E. Mallon, J. Appl. Phys. **47**, 3127 (1976).
[30] D. Shoenberg, *Magnetic Oscillations in Metals* (Cambridge University Press, Cambridge, 1984).
[31] B. Fauqué, N. P. Butch, P. Syers, J. Paglione, S. Wiedmann, A. Collaudin, B. Grena, U. Zeitler, and K. Behnia, Phys. Rev. B **87**, 035133 (2013).
[32] G. Schubert, H. Fehske, L. Fritz, and M. Vojta, Phys. Rev. B **85**, 201105(R) (2012).
[33] H.-M. Guo, G. Rosenberg, G. Refael, and M. Franz, Phys. Rev. Lett. **105**, 216601 (2010).
[34] J. M. Ziman, *Theory of Solids* (Cambridge University Press, Cambridge, 1972), p. 315.